Sentinel-1 snow depth assimilation to improve river discharge estimates in the western European Alps

I. Brangers[1], H. Lievens[2], A. Getirana[3,4], and G. J. M. De Lannoy[1]

[1]Department of Earth and Environmental Sciences, KU Leuven, Heverlee, Belgium
[2]Department of Environment, Ghent University, Ghent, Belgium
[3]Hydrological Sciences Laboratory, NASA Goddard Space Flight Center, Greenbelt, MD, USA
[4]Science Applications International Corporation, Greenbelt, MD, USA

Key Points:

- The assimilation of Sentinel-1 snow depth retrievals reduces the bias in NoahMP snow depth and snow water equivalent estimates.
- The temporal correlation of streamflow simulations increased from 0.61 for the model-only run to 0.73 with the assimilation of Sentinel-1 based snow depth.
- Sentinel-1 based snow depth estimates can be of considerable value for hydrological modeling in mountainous regions.

Corresponding author: Isis Brangers, isis.brangers@kuleuven.be

Abstract

Seasonal snow is an important water source and contributor to river discharge in mountainous regions. Therefore the amount of snow and its distribution are necessary inputs for hydrological modeling. However, the distribution of seasonal snow in mountains has long been uncertain, for lack of consistent, high resolution satellite retrievals over mountains. Recent research has shown the potential of the Sentinel-1 radar satellite to map snow depth at sub-kilometer resolution in mountainous regions. In this study we assimilate these new snow depth retrievals into the Noah-Multiparameterization land surface model using an ensemble Kalman filter for the western European Alps. The land surface model was coupled to the Hydrological Modeling and Analysis Platform to provide simulations of routed river discharge. The results show a reduction in the systematic underestimation of snow depth, going from 38 cm for the open loop (OL) to 11 cm for the data assimilation (DA) experiment. The mean absolute error similarly improves from 44 cm to 37 cm with DA, with an improvement at 59% of the in situ sites. The DA updates in snow depth results in enhanced snow water equivalent and discharge simulations. The systematic negative bias in the OL is mostly resolved, and the median temporal correlation between discharge simulations and measurements increases from 0.61 to 0.73 for the DA. Therefore, our study demonstrates the utility of the S1 snow depth retrievals to improve not only snow depth amounts, but also the snow melt contribution to river discharge, and hydrological modeling in general.

1 Introduction

Snow is an important water resource for people around the globe. It supplies the majority of water for consumption for about a sixth of the world's population during the melting season (Barnett et al., 2005). In the European Alps, snow melt is used by the densely populated downstream regions, providing water for domestic use, agriculture and hydropower generation (Blanc, P., & Schädler, 2014). Knowledge on the amount and distribution of snow is essential for hydrological modeling in mountainous catchments to support water management planning and flood forecasting (Dechant & Moradkhani, 2011; Griessinger et al., 2019; Stigter et al., 2017). Moreover, snow also impacts the surface energy balance by insulating the ground, reflecting incoming radiation and absorbing latent heat during the melt season. A better representation in models would thus also benefit numerical weather prediction (Helmert et al., 2018; de Rosnay et al., 2014).

Land surface models (LSM) can simulate the accumulation and melt of snow throughout the year, providing continuous estimates of snow depth (SD) and snow water equivalent (SWE). However, imperfections in the model physics and forcing data cause these simulations to be uncertain, especially in complex terrain (Krinner et al., 2018; Mortimer et al., 2019). An evaluation by Wrzesien et al. (2017, 2019) of different models and remote sensing products over the United States showed systematic underestimation of modeled SWE. Furthermore, the spread between different models or reanalyses is large (Wrzesien et al., 2017; Mortimer et al., 2019)

SD can also be estimated from in situ or remotely sensed observations. Point scale measurements, however, are not always representative for the surrounding area due to the spatial variability in mountains, in particular in regions where the measuring network is sparse. Estimates of snow cover can be retrieved from satellite observations in the visual or near infra-red spectrum, e.g. from the Moderate Resolution Imaging Spectroradiometer (MODIS) (Hall & Riggs, 2007) or derived from multiple sensors as in the Interactive Multisensor Snow and Ice Mapping System (IMS) (Helfrich et al., 2007), but these products contain no information on the actual snow depth. Passive microwave satellite observations, on the other hand, can provide SD estimates with extensive spatial coverage (Kelly et al., 2003). However, their low spatial resolution (>10 km) and signal saturation in deep snow (Tedesco & Narvekar, 2010) makes them less suitable for applica-

tions in mountain areas. Lidar data such as from the Airborne Snow Observatory (ASO) can be used to retrieve high resolution, high quality SD maps (Painter et al., 2016), but practical and budget constraints limit their use for large scale applications.

The snow science community is currently investigating which type of sensors would be suitable for a new satellite mission focused on the retrieval of snow mass (via SD or directly as SWE), e.g. through NASA's SnowEx campaign (Durand et al., 2017). L-band interferometry experiments have shown promising results (Marshall et al., 2019; Tarricone et al., 2022; Rott et al., 2004; Guneriussen et al., 2001). The potential of Ku- and X-band sensors has been supported by both experimental and modeling studies (Tsang et al., 2021). All these radar technologies show potential to deliver a viable SD or SWE product in the future, but they are not operationally available yet.

In the meantime, a study by Lievens et al. (2019) has shown the potential of the Sentinel-1 (S1) C-band (5.4 GHz) radar satellite to provide SD estimates at sub weekly time steps and 1 km spatial resolution. The usability of C-band for snow mass has long been put aside after experiments with co-polarized backscatter had shown limited sensitivity (Bernier & Fortin, 1998; Pivot, 2012). The recent study of Lievens et al. (2019) differs from previous work by focusing on cross-polarized backscatter and deeper snowpacks. Their SD retrieval algorithm is based on an empirical change detection approach of the ratio between cross-polarized an co-polarized backscatter, and performs best for deeper snowpacks. The retrievals only work for dry snow and are more uncertain in the case of shallow snow and higher forest cover. According to the current physical understanding, the S1 SD retrieval is based on the fact that a growing snowpack leads to an increase in scattering. Since the size of individual snow grains is small compared to C-band wavelength ($\sim$5 cm), the scattering is more likely to originate from clusters of grains, multiple scattering between layer interfaces, snow-ground interactions or other snow structures (Tsang et al., 2021). More research is being done to expand the underlying scattering theory.

Continuous and improved SWE or SD estimates can be obtained through the assimilation of snow observations into LSMs. In the absence of satellite based SD retrievals, operational models often make use of in situ SD or SWE measurements added through interpolation schemes, snow cover (SC) observations or a combination of both (de Rosnay et al., 2014; de Rosnay et al., 2015; Helmert et al., 2018; Magnusson et al., 2014). Charrois et al. (2016); Revuelto et al. (2021) have shown modeled SD can be improved by assimilating spectral reflectance data. Derived SC observations have also shown to improve model performance (Stigter et al., 2017; Margulis et al., 2016; Toure et al., 2018; Largeron et al., 2020), and can be further converted into SWE using snow depletion curves (Oaida et al., 2019; Andreadis & Lettenmaier, 2006; Arsenault et al., 2013). However, visual light imagery has the disadvantage of being limited to cloud-free situations and contains no direct information on the snow mass itself. Other studies have assimilated satellite-based SD from passive microwave observations, but with limited success. The Advanced Microwave Scanning Radiometer for EOS (AMSR-E) estimates have a coarse resolution, tend to saturate for deeper snowpacks and are unable to capture the observed interannual variability (Andreadis & Lettenmaier, 2006; De Lannoy et al., 2012). Alternatively, optical or microwave signals can be assimilated to improve snowpack estimates (Durand & Margulis, 2006; Alfieri et al., 2022).

Snow data assimilation has been performed using various methods. The simplest method is through direct insertion (Hedrick et al., 2018), however this does not take into account relative model and observation uncertainties (Arsenault et al., 2013). A widely used and statistically more optimal scheme is the Ensemble Kalman Filter (EnKF) (Evensen, 2003). In the EnKF, the model uncertainty is estimated from the spread of an ensemble of model trajectories (Reichle, 2008). Although the underlying assumptions of unbiased, normally distributed errors are often lightly violated, the methodology has been shown to be robust (Reichle et al., 2002) and has been applied widely and successfully

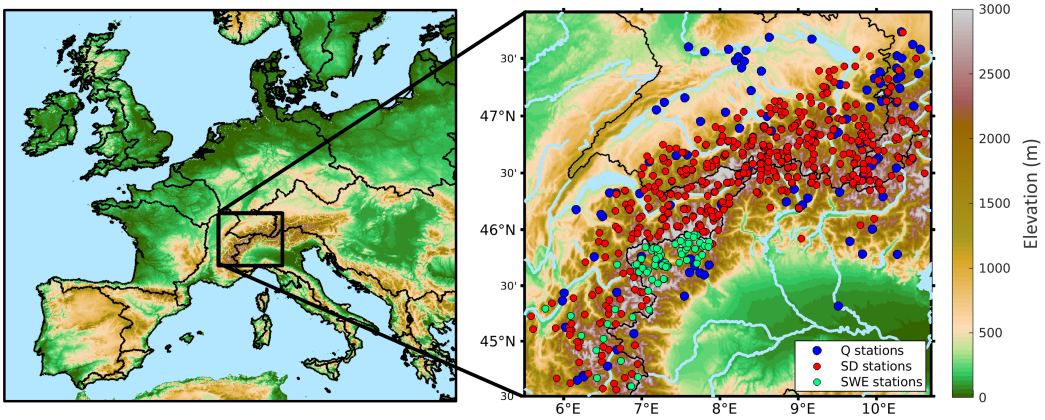

Figure 1. Location of the research area in the European Alps. The black lines delineate the main drainage basins. The blue and red dots indicate the stations with discharge (Q, n=105) and snow depth (SD, n=532) measurements respectively.

in assimilation studies for snow (Arsenault et al., 2013; De Lannoy et al., 2010; Magnusson et al., 2014; Andreadis & Lettenmaier, 2006) and its coupling to hydrology (Sun et al., 2004; Stigter et al., 2017). More recently, particle filters have received more attention (Magnusson et al., 2017; Piazzi et al., 2018). This methodology requires no assumptions on the model or observation distribution and can therefore be a good alternative for the EnKF in strongly nonlinear systems (Gordon et al., 1993). For this study, the model runs were performed using NASA's land information system (LIS), a modeling framework which combines different types of models, observations and data assimilation methods (Kumar et al., 2006). LIS has been used for multiple previous snow DA studies (e.g. Kumar et al., 2015; De Lannoy et al., 2012; Park et al., 2022; Cho et al., 2022).

In this study, we investigate the effectiveness of the new S1 SD estimates in a practical application. Over a selected research area of the western European Alps we assimilate the S1 based SD observations into a coupled land surface and routing model using an Ensemble Kalman Filter. The goal is to quantify to which extent SD data assimilation can improve model simulations of SD, SWE and river discharge. Therefore, the model output with and without assimilation has been compared to reference data, consisting of point scale SD, SWE and river discharge measurements from different networks across the region.

2 Materials and Methods

2.1 Study region

The research domain is presented in Figure 1 and covers the western European Alps, specifically from 44.0°N to 47.8°N and 5.5°W to 10.7°W. This region is of considerable hydrological importance, containing the upper catchments of some of Europe's major rivers, including the Rhone, the Rhine, the Danube and the Po. The study area covers a wide range of land cover types, slopes, aspects and elevations.

2.2 Sentinel-1 snow depth observations

C-band (5.4 GHz) radar backscatter measurements from the ESA and Copernicus S1 constellation were processed over the Alps for the period September 2015 through August 2021. The raw data was processed using the ESA Sentinel Application Platform (SNAP)

toolbox to γ^0 (in dB) as in Lievens et al. (2022). The first empirical algorithm to turn changes in backscatter into SD was applied over the Northern Hemisphere mountains at 1 km resolution in Lievens et al. (2019). The method was further improved and applied at 100 m, 500 m and 1 km resolutions over the European Alps in Lievens et al. (2022). This current work makes use of the retrievals from the latter study at the 1 km resolution, approximating the 0.01° latitude-longitude model simulation grid to which the retrievals were interpolated using nearest neighbour sampling. Before the launch of Sentinel-1B in April 2016 less frequent S1 observations are available than during the rest of the period. This makes the earlier SD retrievals more prone to noise, which could adversely impact the data assimilation performance.

The Sentinel-1 snow depth retrieval algorithm is based on an empirical change detection algorithm applied to γ^0_{VH} and γ^0_{VV} radar backscatter. The presence of liquid water during melt causes a strong decrease in γ^0, which increases the uncertainty in the associated SD retrievals. A wet snow detection mechanism has been included in the retrieval algorithm (Lievens et al., 2022), which allows for masking the S1 SD observations in wet snow conditions. Observations are masked when the backscatter difference between an observations and the previous observation from the same relative orbit is larger than 2 dB.

S1 SD estimates are available until April, but we noticed that omitting observations from March onwards led to better data assimilation results. The wet snow detection algorithm sometimes misses the onset of snow melt, especially if the backscatter decreases gradually. By refraining from assimilating observations from March onwards, we can limit the potential negative impacts from missed wet snow presence. The retrievals are thus assimilated during the months August through February according to the availability and coverage of the S1 acquisitions. Over the Alps, observations are typically available every ±3 days.

The S1 based SDs show very good correspondence to in situ measurements and are able to realistically represent spatial and temporal variability. Compared to in situ measurements, the mean relative errors are 20-30% of the in situ measured SD, for SD values between 1.5 and 3 m. Higher uncertainties were found in regions with shallow snow or dense forest cover (Lievens et al., 2022).

2.3 Noah MP 3.6 and HyMAP

To simulate processes at the land surface, we used the Noah land surface model with multiparameterization options version 3.6 (NoahMP) (Niu et al., 2011). Given meteorological forcings, such as precipitation and radiation, and land surface characteristics, such as elevation, land cover and soil texture, the model simulates surface and subsurface processes. This leads to continuous estimates of the model state variables, including soil moisture, soil temperature, SD, SWE, and fluxes, including surface and sub-surface runoff. In NoahMP the snowpack processes are represented by a detailed physically-based parametrization, including multiple snow layers, melt-freeze processes and canopy snow interception. In comparison with the previous model version, the Noah LSM, the simulation of runoff within NoahMP is improved by the introduction of permeable frozen soils and the simulation of snow melt is more accurate (Niu et al., 2011). In NoahMP, glaciers are not explicitly simulated, but are simply represented by the land cover class of ice. This static land cover cannot provide any melt water contribution other than that of the seasonal snow falling on top. Therefore, catchments that are considerably impacted by glacial meltwater were excluded from this study.

NoahMP is coupled to the Hydrological Modeling and Analysis Platform (HyMAP) (Getirana et al., 2012; Getirana, Peters-Lidard, et al., 2017). HyMAP is a global river routing scheme that uses the LSM's surface and sub-surface runoff estimates as input to simulate horizontal water fluxes. In this study, HyMAP was setup with the kinematic

wave equation with optimal sub timesteps determined with the Courant–Freidrichs–Levy (CFL) condition (Courant et al., 1967). River flow is routed between grid cells through a prescribed river network as in Getirana et al. (2012). HyMAP has been thoroughly validated over the Amazon basin (Getirana et al., 2012) and has been applied across the globe for various studies (Getirana, Kumar, et al., 2017; Jung et al., 2017) including a study about the assimilation of SC and SD into an LSM (Kumar et al., 2015).

2.4 Model-only and data assimilation experiments

Within NASA LIS, NoahMP ran on a grid of 0.01° resolution with the parametrization options as in Kwon et al. (2019). The configuration also closely resembles the study of Park et al. (2022), that assimilated S1 backscatter in NoahMP over Western Colorado, but here we assimilate S1 derived SD instead of the backscatter itself. The model was forced with meteorological input data from the Modern-Era Retrospective analysis for Research and Applications, version 2 (MERRA-2) (Gelaro et al., 2017). The precipitation data from MERRA-2 has been bias corrected with gauge-based precipitation observations (Reichle et al., 2017). The low resolution (0.5°) MERRA-2 forcings were downscaled to the finer model grid by applying bilinear spatial interpolation with a topographic lapse-rate correction. Before starting the assimilation experiments, NoahMP was run for 20 years (1995-2015) as a spin-up. Then, for the period from September 2015 through August 2021 two ensemble runs were performed: first, an open loop run without assimilation as a benchmark; second, a run with assimilation of S1 SD observations. The model was run at 15-min time steps, whereas daily averaged outputs were saved and analyzed.

The updates of the snow state variables were performed with a one-dimensional ensemble Kalman filter (Reichle et al., 2002). During the analysis step, the modeled SD and SWE are locally pulled more or less towards the observations depending on the uncertainties in the model forecasts and observations. The uncertainty of the S1 SD observations is estimated as 30 cm, and is assumed to be constant in space and time. The uncertainty of the model forecast is estimated by perturbing selected state variables (SD and SWE) and forcings (precipitation, longwave and shortwave radiation) in 12 ensemble members (see Table 1). Compared to the older Noah LSM, NoahMP simulates a snowpack with multiple snow layers of variable depth. To conserve the snow density of the different layers during the analysis, the updates were divided over the layers proportionate to their share of the total SWE.

Unlike some earlier snow data assimilation studies (e.g. De Lannoy et al. (2012)), the SD retrievals are not rescaled to the model climatology in this study, even if biases between both are found. However, since snow is a cumulative variable, any instantaneous error can lead to persistent bias and any filter update can correct for it with a lasting effect. Furthermore, comparison with in situ measurements have shown S1 to be mostly unbiased and the model systematically underestimating SD, especially for the higher SD values. By not a priori rescaling the SD observations to the model climatology, we are able to counter model bias, even if a bias-blind data assimilation system might be suboptimal (Dee, 2006).

2.5 Validation

The daily SD and streamflow outputs of the model runs were compared to point scale observations from different in situ networks. The SD data was provided by Météo-France and the WSL Institute for Snow and Avalanche Research SLF. SWE data was provided by Electricité de France and ARPA Valle d'Aosta. Of the 68 SWE stations, 17 are automatic stations with daily observations, the others provide biweekly observations. Daily streamflow data were collected from various local instances, specifically Eaufrance (France), eHYD (Austria), Federal Office for the Environment (Switzerland), Gewässerkundlicher Dienst Bayern (Germany), Landesanstalt für Umwelt Baden-Württemberg (Germany),

Table 1. Perturbation parameters applied for the OL and DA runs (with M=multiplicative, A=additive, Std=standard deviation, Tcorr=temporal autocorrelation, Xcorr=cross-correlations).

State/Forcing	**Type**	**Std**	**Tcorr**	**Xcorr**		
Snow depth	M	0.0005	3 hours	1	0.9	
SWE	M	0.0005	3 hours	0.9	1	
Precipitation	M	0.5	1 day	1	-0.8	0.5
Shortwave radiation	M	0.3	1 day	-0.8	1	-0.5
Longwave radiation	A	50 W/m^2	1 day	0.5	-0.5	1

Agenzia Regionale per la Protezione Ambientale - ARPA Lombardia (Italy), ARPA Piemonte (Italy) and ARPA Valle d'Aosta (Italy). Reference data of daily precipitation was acquired from MeteoSwiss. In total we used 532 stations for SD, of which 460 above 1000 m elevation, 105 stations for discharge, 68 stations for SWE and 603 for precipitation validation (see Figure 1).

First, the in situ SD and SWE measurements were compared to the modeled SD and SWE from the OL and DA runs. Improvements were quantified in terms of conventional metrics like temporal correlation (R; dimensionless), mean absolute error (MAE; in m) and bias (in m). Timesteps with in situ SD = 0 cm were excluded from the calculation of the metrics, but were included when plotting the time series of mean SD or SWE. To focus on sites impacted most by the snow DA, stations with a maximal in situ SD below 25 cm were removed, as were stations without S1 observations. In situ SD stations are typically located in flat areas that are relatively easily accessible. The network in the region of study is relatively dense, however the highest mountain peaks are underrepresented in the analysis. The impact of SD assimilation at the highest elevations can still be determined indirectly through the impact on river discharge.

Second, the OL and DA streamflow estimates were compared with in situ measurements. With a better representation of the snow state, we expect improvements in the DA runoff volume during the melting season, and thus a better representation of peak flow. We calculated the validation metrics only for the melting season (chosen as February through September), when most impact of SD retrieval DA is expected. We excluded stations with low flows ($< 1\,\mathrm{m}^3/\mathrm{s}$) and less than 100 days of data. Another necessary quality control measure was to manually remove discharge stations that are considerably influenced by glaciers, since NoahMP is not able to estimate glacier melt (manual selection based on glacier cover fraction), and to remove basins that are largely impacted by dams. These constraints strongly limited the amount of available stations, but are necessary to ensure the quality of the analysis. The 105 remaining stations measure the flow from basins of variable size and elevation, and are assumed to be a representative sample. The considered metrics are the time series correlation, the normalized mean absolute error (MAE; dimensionless) and the total volume error (DV; dimensionless). The MAE was normalized by the mean observed flow to allow for comparison of rivers of different sizes. The total volume error shows the fraction of under- or overestimation of the total discharge volume during the melting season, independent of daily fluctuations. It was calculated per station, as follows:

$$\mathrm{DV} = \frac{\sum_{i=1}^{n} \mathrm{sim}_i - \sum_{i=1}^{n} \mathrm{obs}_i}{\sum_{i=1}^{n} \mathrm{obs}_i}$$

with n equaling the number of observations, obs_i the in situ observations, and sim_i the simulated (OL or DA) discharge for time steps $i = 1, \ldots, n$.

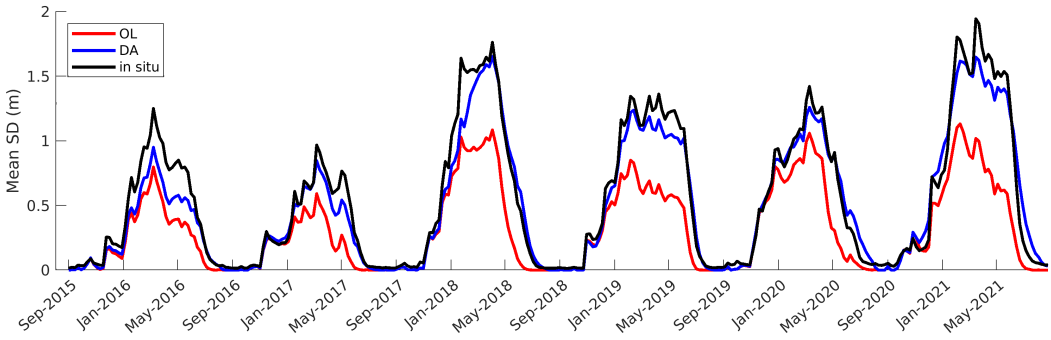

Figure 2. Time series of weekly SD (m) mean over all in situ SD stations (n=532).

3 Results and Discussion

3.1 Snow depth and SWE

We evaluated the effect of the S1 SD assimilation on the time series of SD across the study area. As one can see in the timeseries of mean spatial SD in Figure 2, the model only run (OL) performs quite well in reproducing the seasonal trend of accumulation of the snowpack, and is able to simulate the interannual variability (anomaly R = 0.69). However, it systematically underestimates the SD compared to in situ observations, causing an unrealistically early melt onset. On average, the S1 DA causes the model to be pulled upwards closer to the in situ observations. The reduced bias furthermore results in an improved representation of the snow melt. The generally deeper DA snowpack requires more energy and thus takes more time to melt.

For each of the stations above 1000 m (n=460), the SD time series R, MAE and bias were calculated (zero SD values excluded). The distribution of the metrics is show in Figure 3. The DA strongly reduces the bias from -27 cm to -6 cm. This does, however, not translate into an improved correlation with in situ measurements. The correlation remains unchanged at 0.83, which can likely by attributed to two counteracting effects. On the one hand, the reduction in bias causes the timing of the melt season to be represented better. On the other hand, noisy satellite observations, and the gradual correction towards the observations distorts the seasonal trend in snow accumulation. The MAE remains mostly unchanged, with only a marginal improvement. The violin shape indicates that after DA there are less sites with high MAE, but also less sites with very low MAE. Anomaly correlations slightly decrease from R_{an}=0.69 for the OL run to 0.59 for the DA run (not shown), because the filter updates inevitably introduce unnatural short-term variability.

The S1 SD observations are translated to updates in both the SD and SWE state variables. Figure 4 shows timeseries of SWE and SD along with the ensemble standard deviation for a single station in the French Alps. The state perturbations are multiplicative, causing a larger model spread in case of higher SD or SWE. The model uncertainty, and thereby the weight on the observations, increases along the season with the accumulation of snow. The observation uncertainty is considered constant at 30 cm throughout the season. Future research could optimize the spatiotemporal representation of the observation uncertainty.

Figure 5 shows the relationship between modeled and in situ SD or SWE for all validation points in space and time. The spatiotemporal metrics displayed on the figure differ from the site-based temporal metrics in Figure 3. For the latter figure, sites were limited to elevations above >1000 m. Similar to the previous results, the OL run

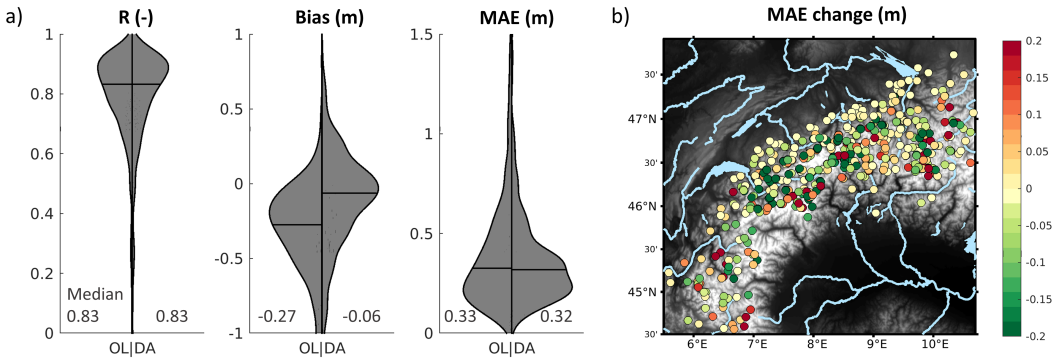

Figure 3. SD performance. a) Plots showing the distribution of station performance for chosen metrics. The metrics are calculated for all stations above 1000 m (n=461) excluding timesteps with in situ SD=0 cm. b) Change in MAE (DA-OL) for all stations (n=532) in the study area.

shows a bias in SD. The underestimation gradually increases with higher SD values. The patterns are consistent between the SD and SWE data, indicating no major issues with modeled snow densities. In the DA experiment, the biases in SD and SWE are strongly reduced, with a bias of -38 cm for the OL to -12 cm for the DA run.

The spatial distribution of SD for the OL and DA results is mapped in Figure 6 for February 2019. The spatial pattern in the OL run is relatively uniform and does not well represent the variability and range that are expected in high mountain regions. This might be caused by the low resolution of the meteorological input, a sub-optimal forcing interpolation scheme or other imperfections in the model and forcing data. Potential limitations of the meteorological forcings are further discussed in section 3.3. By assimilating the S1 SD retrievals, it is possible to derive a more realistic spatial distribution in SD (Figure 6c). To verify this, the spatial correlation was calculated per month and is presented in a time series in Figure 7. The figure indicates a minor degradation in spatial correlation with DA, except during the melt season. The scatter plot of in situ versus modeled SD in Figure 7b shows an increased spatial variability of the DA compared to the OL. The DA leads to a substantial reduction in bias (closer to the diagonal), but with a wider spread.

Figure 8 further elaborates on the DA performance. Figure 8a demonstrates improved DA results (quantified as a change in MAE relative to the OL) in case of high OL error and low S1 error, and worse DA results case of low OL error and high S1 error. This is an indication that the DA system is working as expected. The figure also shows the complementarity of S1 and the model, with OL and S1 performing relatively better at different sites. Figure 8b shows a relationship between OL and S1 bias. The S1 SD estimates are based on remote sensing data only, and are created independently of the model run. Nevertheless, a relationship between the OL and S1 biases is found. That is, sites for which a larger bias is observed in the OL simulations typically also feature a larger bias in the S1 retrievals. This can likely be attributed to in situ stations that are not representative for the larger 1 km pixel they are assumed to portray. When comparing relatively coarse scale data in mountainous terrain with point scale sites, some representativity issues are to be expected and are hard to avoid.

Figure 8c shows the change in MAE relative to the mean site SD. The sites with the highest in situ snow depths coincide with the sites with the most underestimated OL simulations. Here the DA has the largest potential for improvement. However, the opposite is true for the sites with lower observed SD's. There, the OL is mostly unbiased and the MAE is deteriorated by the assimilation of S1 SD. From previous work, S1 ob-

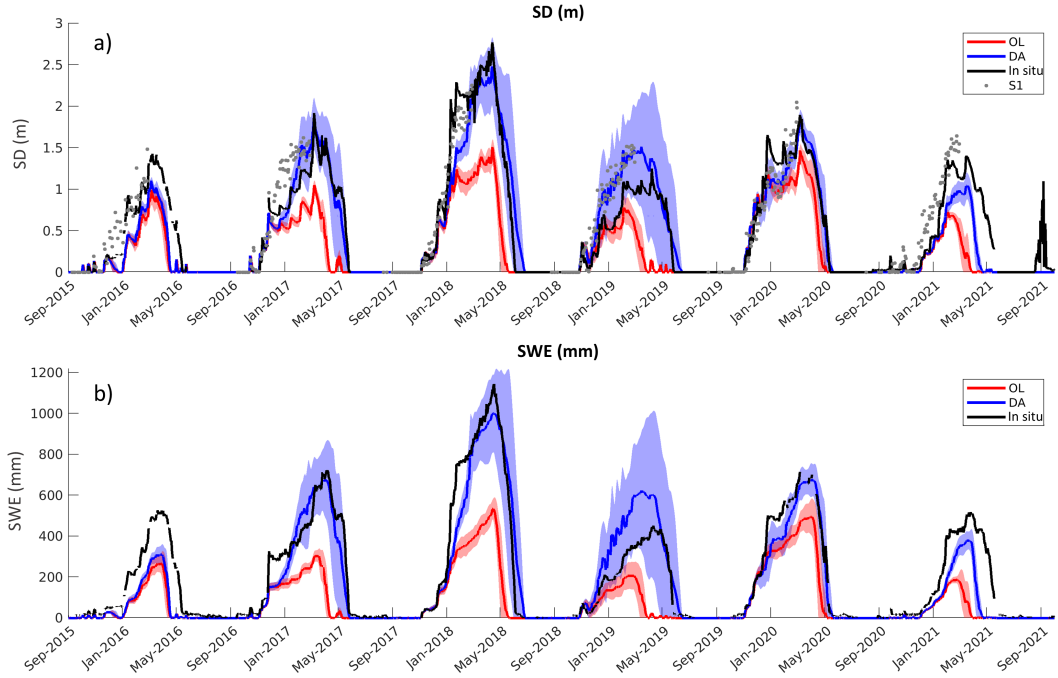

Figure 4. Timeseries of (a) SD (m) and (b) SWE (mm) for a station in the French Alps (45.22°N 6.88°E). The range of ensemble members is shown by the shaded area surrounding the mean.

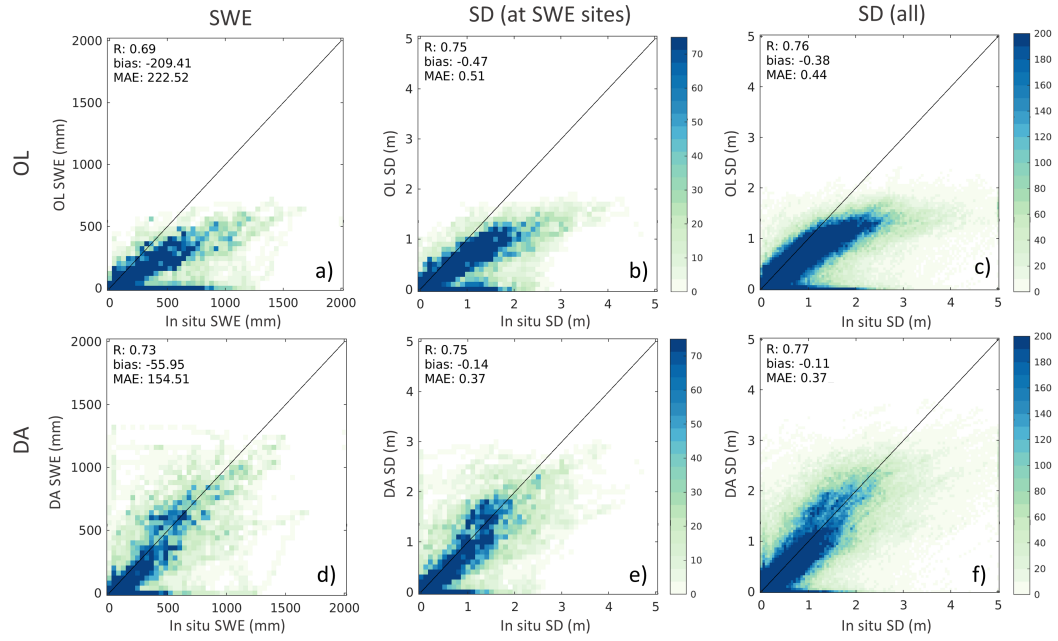

Figure 5. Density plots showing the relationship between simulated and in situ SD and SWE for all sites and timesteps: (a, b, c) OL, and (d, e, f) DA. Zero values were masked, leaving 27 376 observations for SWE (MAE and bias given in mm) and 455 637 observations for SD (MAE and bias given in m).

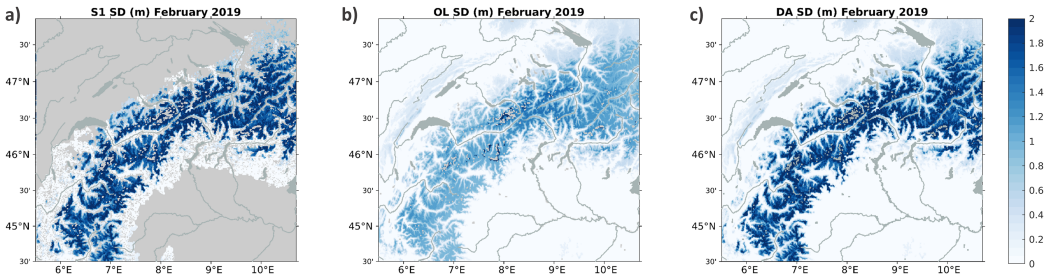

Figure 6. Mean snow depth (m) in February 2019 for (a) S1 retrievals, (b) the model-only run, and (c) the data assimilation run.

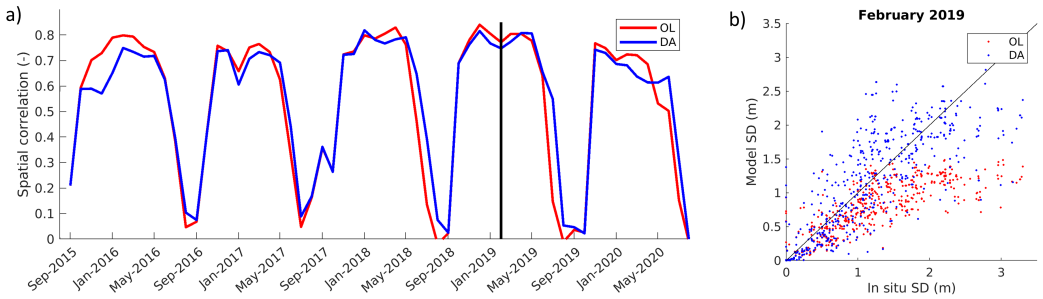

Figure 7. Spatial correlation of SD. a) Time series of spatial correlation of monthly averaged SD (including zeros). The black line indicates the time step that was used for the scatter plot. b) Scatter plot of in situ vs modeled SD for February 2019 (n=532).

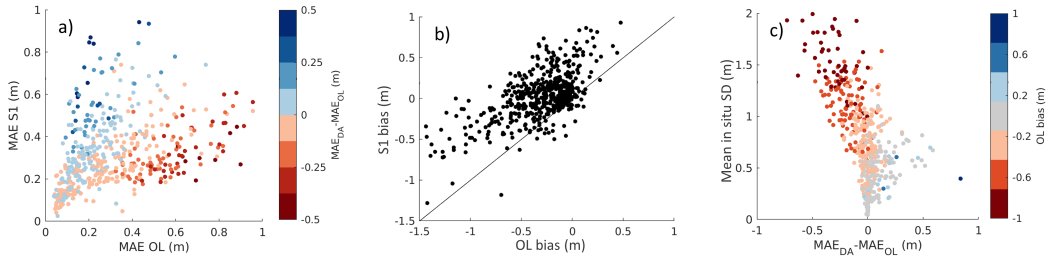

Figure 8. Distribution of station-based performance metrics (n=532). a) DA improvement in MAE relative to the OL and S1 performance. b) Relationship between the OL and S1 biases. c) Improvement in model performance (MAE) related to the mean site SD and the OL bias.

servations are known to perform best at the higher elevations with deep dry snow (Lievens et al., 2022). Thus for this model setup the S1 based SD observations are working best where they are most needed i.e. at high elevations.

3.2 Discharge

We also evaluated the impact of the SD assimilation on the simulation of river discharge. The discharge is an integrated measurement of water flow from an entire basin, and since in situ SD measurement sites are scarce, an evaluation in terms of discharge can give a more complete assessment of the added value of the S1 SD retrievals. Figure 9 shows the distribution of performance metrics for the discharge stations. The metrics

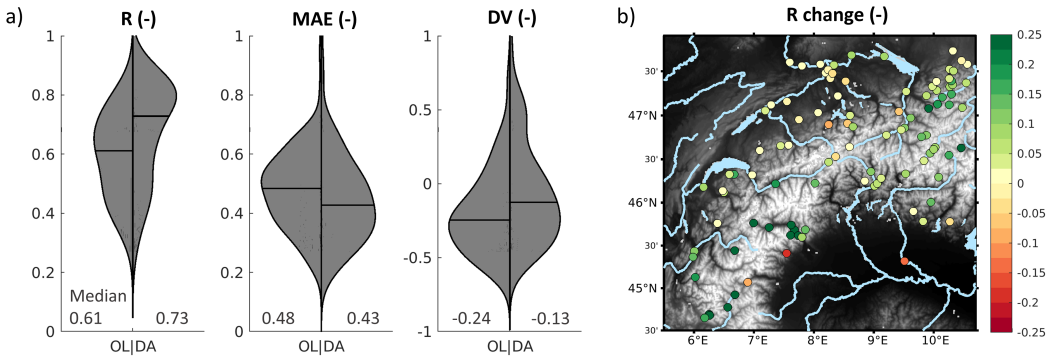

Figure 9. River discharge performance. a) The violin plots with the distribution of the performance metrics for the used discharge stations (n=105). The MAE and DV were normalized by the mean observed flow and total observed flow respectively. All metrics are unitless and are calculated for the melting season only (February-September). b) Change in R (DA-OL) for the different stations in the study area.

were calculated for the melt season only (February-September). In our analysis, the DA run was found to outperform the OL for all metrics. The median R improves from 0.61 to 0.73, meaning that the seasonal variability of discharge is represented more accurately. To illustrate this, two time series with a clear improvement in the timing of peak discharge are shown in Figure 10. Similar to the bias in SD, the total volume of discharge is underestimated in the OL by $\sim 24\%$ of the total observed flow. The latter is partly corrected by the DA, reducing the negative bias to $\sim 13\%$ of the total flow. For instance, in the time series in Figure 10, the OL flow is underestimated during the melt period, and the shape is distorted. After assimilation of S1 SD, the snow melt contribution to the streamflow is simulated more realistically. The improved snow distribution in the model, especially the addition of snow at the highest elevations, leads to a delay in peak flow. Deeper snow packs have a higher energy requirement before reaching isothermal conditions and melt onset. We therefore assume the improvements in the discharge can be attributed mostly to fixing the snow bias into more realistic peak SWE amounts.

Our results show how some of the shortcomings of the model (input) can be corrected with qualitative SD estimates. Similarly, recent work from Alfieri et al. (2022) found a 4% KGE improvement in river discharge by assimilating S1 SD estimates in a hydrological model for the Po valley. Park et al. (2022) assimilated the raw Sentinel-1 backscatter in a model setup similar to this current study. Their results showed improvements in SWE, with R increasing from 0.75 to 0.80, and slight improvements for river discharge for an area in western Colorado.

3.3 SD bias and precipitation

Figure 3 and 5 showed that the SD is systematically underestimated in the OL NoahMP simulations. Wrzesien et al. (2019) found a similar underestimation of SD using NoahMP in North American catchments using multiple meteorological forcings, including MERRA-2. They attributed the underestimation to errors in the forcing inputs. To verify if this was also the case in our experiment, we compared the total precipitation as used in the model with data from 603 in situ precipitation gauges in Switzerland. The total precipitation used here refers to the bias corrected MERRA-2 precipitation (Reichle et al., 2017) with a bilinear spatial interpolation applied to downscale to the model grid. The forcings like air temperature and pressure are adjusted for the elevation with a lapse-rate

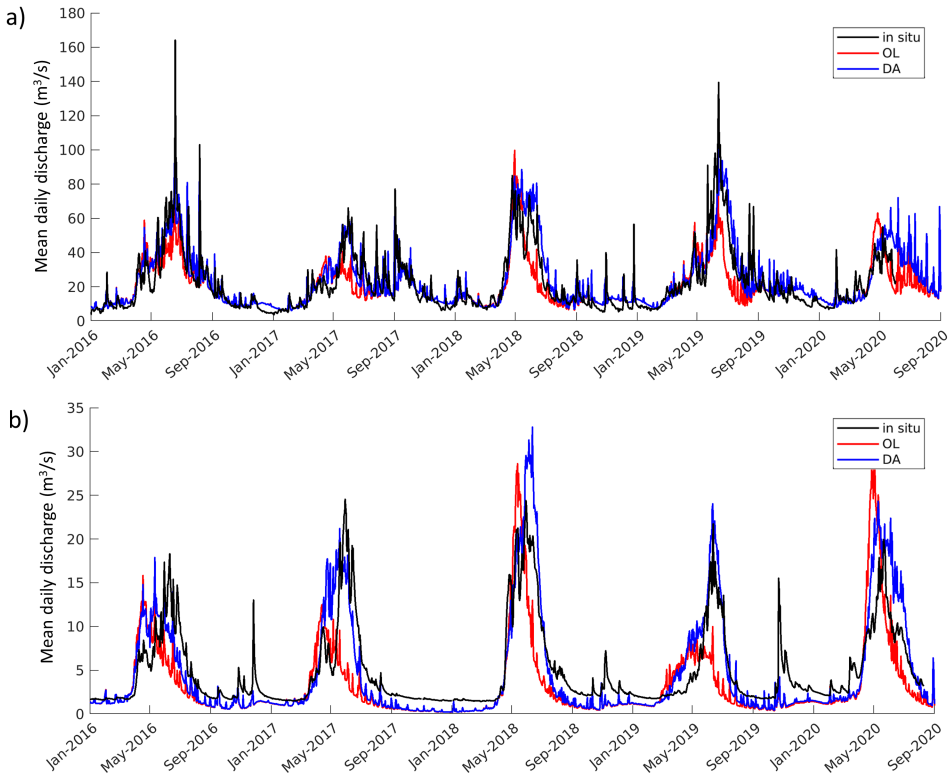

Figure 10. Time series of discharge at two stations, showing the impact of the S1 SD assimilation on river discharge. a) Landquart, Switzerland (46.97°N 9.61°E), b) La Durance, France (44.92°N 6.68°E).

correction (Cosgrove et al., 2003). This impacts the partitioning of precipitation between snow and rain, but otherwise no elevation correction is applied to the precipitation itself. Orographic effects that could play a significant role in the distribution of precipitation throughout the MERRA-2 pixels are not taken into account. To compare the amount of solid precipitation, the total precipitation of both the model and the in-situ stations were multiplied with the model derived ice fraction (derived as in Jordan (1991)).

Contrary to our expectations, the analysis did not show a systematic underestimation of precipitation by MERRA-2. Figure 11 even shows that MERRA-2 slightly overestimates the accumulated precipitation compared to in situ measurements. The mean end of season accumulated precipitation was 14% higher for MERRA-2 than for the in situ measurements. For snowfall only, the estimates were mostly unbiased. However, it is important to note that automated measurements tend to underestimate the amount of precipitation, especially snow, depending on the type of gauges used and the wind speed (Grossi et al., 2017). Rasmussen et al. (2012) mentions errors from 20 to 50% for solid precipitation. It is thus possible that the precipitation forcing is slightly low biased even though the comparison with in situ stations does not indicate this. When looking at individual precipitation events in Figure 11b, MERRA-2 was found to favor smaller and more moderate rainfall events and underestimates storms. This can be expected due to the coarse resolution of the input, spreading out local storms onto larger regions. Although precipitation information at the highest elevations is lacking, no clear trend between accumulation bias and elevation was found (Figure 11c).

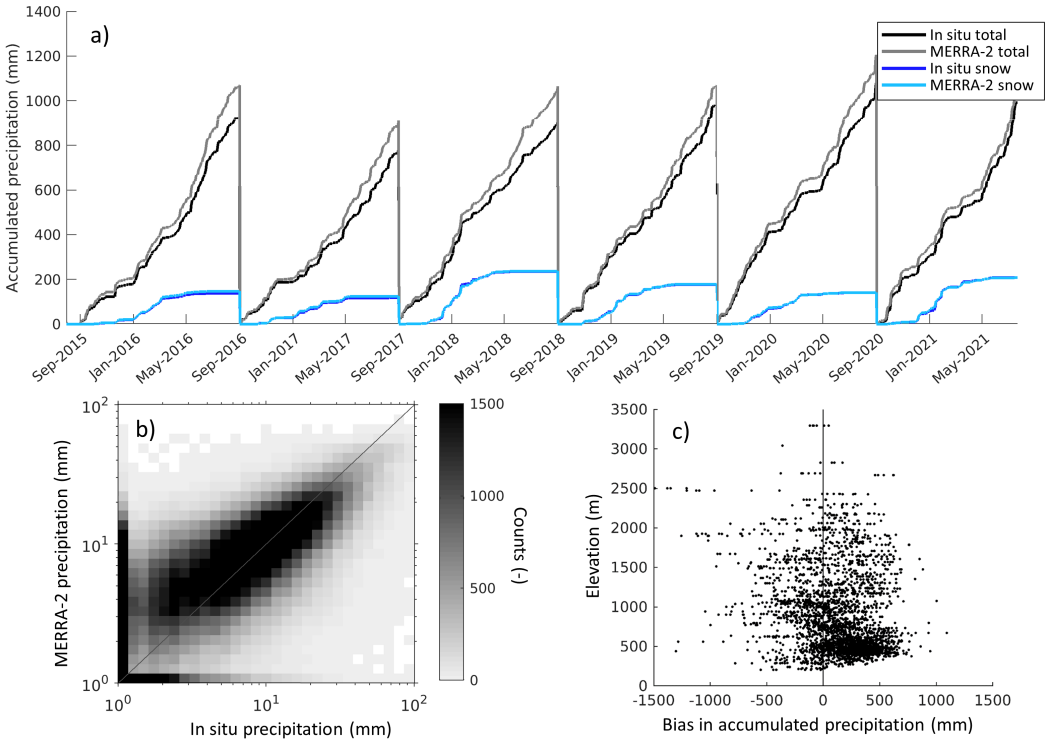

Figure 11. Validation of MERRA-2 bias corrected precipitation with in situ data. (a) Time series of the mean accumulated precipitation over all stations (n=603). (b) Density plot comparing in situ and MERRA-2 precipitation of individual rainfall events. (c) Bias in end of season accumulated precipitation stratified by elevation.

Next to flaws in the forcing data, errors can also be caused by inaccuracies in model parametrizations like the rain-snow partitioning, snow density evolution, albedo, heat exchange, sublimation or melt-freeze dynamics. A more thorough analysis of the precipitation, the water balance and model structure is needed to identify the cause of the systematic underestimation in SD in NoahMP forced by MERRA-2. Once a faulty parameter could be identified, it should be included in the update vector of the DA experiment to improve the results and construct a more robust assimilation system.

4 Conclusions

In this study we investigated the potential of S1-based snow depth retrievals to improve model simulations of SD, SWE and river discharge. Specifically, 1-km resolution S1 SD retrievals were assimilated into the NoahMP LSM version 3.6 coupled to the HyMAP river routing model using an EnKF scheme. The results were validated by comparing the model output to in situ measurements of SD, SWE and river discharge. Compared to the model-only run, the DA simulation significantly reduced the bias in SD (from -38 cm to -11 cm) and SWE (from -209 mm to -56 mm). The MAE improved at 59% of the in situ sites. The impact on R was limited. Sites with shallow snow showed a small deterioration after the assimilation of S1 SD, whereas sites with deep snow featured mostly improvements. The updates in the spatial snow distribution also had a positive impact on the discharge simulations of the studied basins. With the S1 SD DA, we obtained a better representation of the timing (R from 0.61 for OL to 0.73 for DA) and amount of discharge (DV from -24% to -13%) during the snow melt period. The results could dif-

fer for a different region, model or forcing setup. A limitation of our model setup (NoahMP forced with MERRA-2 bias corrected precipitation) was that it led to systematically biased SD estimates. A comparison with precipitation measurements however could not attribute the SD bias to an underestimation in the amount of precipitation. Identifying the cause of this bias and resolving it requires further research.

For this work we used a globally applicable setup without parameter calibration. This makes the setup easily extendable to other domains. The improvements in SD and discharge with the S1 SD DA are encouraging. It shows how high resolution S1-based SD estimates can be useful in hydrological modeling applications, offering a new tool to support operational river forecasting and water management.

Open Research Section

The LSM runs and DA were executed using NASA's LIS platform, which is available on GitHub. Compared to the NASA master, routines were introduced to read S1 SD data, and adjustments were made to the NoahMP3.6 SD DA routine. The GitHub fork with updated routines will be added here after review, and the output will be uploaded on Zenodo.

Acknowledgments

This research is performed within the framework of the BELSPO projects SNOPOST and C-SNOW (SR/01/375). I. Brangers was funded through the Research Foundation Flanders (FWO). The computer resources and services used for Sentinel-1 data processing were provided by the Flemish Supercomputer Center (VSC), funded by FWO, the Flemish Government and KU Leuven C1 (C14/21/057).

References

Alfieri, L., Avanzi, F., Delogu, F., Gabellani, S., Bruno, G., Campo, L., ... Brocca, L. (2022). High-resolution satellite products improve hydrological modeling in northern italy. *Hydrology and Earth System Sciences*, *26*(14), 3921–3939. Retrieved from `https://hess.copernicus.org/articles/26/3921/2022/` doi: 10.5194/hess-26-3921-2022

Andreadis, K. M., & Lettenmaier, D. P. (2006). Assimilating remotely sensed snow observations into a macroscale hydrology model. *Advances in Water Resources*, *29*(6), 872–886. doi: 10.1016/j.advwatres.2005.08.004

Arsenault, K. R., Houser, P. R., De Lannoy, G. J., & Dirmeyer, P. A. (2013). Impacts of snow cover fraction data assimilation on modeled energy and moisture budgets. *Journal of Geophysical Research Atmospheres*, *118*(14), 7489–7504. doi: 10.1002/jgrd.50542

Barnett, T. P., Adam, J. C., & Lettenmaier, D. P. (2005). Potential impacts of a warming climate on water availability in snow-dominated regions. *Nature*, *438*(November), 303–309. doi: 10.1038/nature04141

Bernier, M., & Fortin, J. P. (1998). The potential of times series of C-Band SAR data to monitor dry and shallow snow cover. *IEEE Transactions on Geoscience and Remote Sensing*, *36*(1), 226–243. doi: 10.1109/36.655332

Blanc, P., & Schädler, B. (2014). Water in Switzerland - an Overview. *Bern: Swiss Hydrological Comission*.

Charrois, L., Cosme, E., Dumont, M., Lafaysse, M., Morin, S., Libois, Q., & Picard, G. (2016). On the assimilation of optical reflectances and snow depth observations into a detailed snowpack model. *The Cryosphere*, *10*(3), 1021–1038. Retrieved from `https://tc.copernicus.org/articles/10/1021/2016/` doi: 10.5194/tc-10-1021-2016

Cho, E., Vuyovich, C. M., Kumar, S. V., Wrzesien, M. L., & Kim, R. S. (2022). Evaluating the utility of active microwave observations as a snow mission concept using observing system simulation experiments. *The Cryosphere Discussions*, *2022*, 1–24. Retrieved from `https://tc.copernicus.org/preprints/tc-2022-220/` doi: 10.5194/tc-2022-220

Cosgrove, B. A., Lohmann, D., Mitchell, K. E., Houser, P. R., Wood, E. F., Schaake, J. C., ... Meng, J. (2003). Real-time and retrospective forcing in the North American Land Data Assimilation System (NLDAS) project. *Journal of Geophysical Research: Atmospheres*, *108*(22). doi: 10.1029/2002jd003118

Courant, R., Friedrichs, K., & Lewy, H. (1967). On the partial difference equations of mathematical physics. *IBM Journal of Research and Development*, *11*(2), 215-234. doi: 10.1147/rd.112.0215

De Lannoy, G. J., Reichle, R. H., Arsenault, K. R., Houser, P. R., Kumar, S., Verhoest, N. E., & Pauwels, V. R. (2012). Multiscale assimilation of Advanced Microwave Scanning Radiometer-EOS snow water equivalent and Moderate Resolution Imaging Spectroradiometer snow cover fraction observations in northern Colorado. *Water Resources Research*, *48*(1), 1–17. doi: 10.1029/2011WR010588

De Lannoy, G. J., Reichle, R. H., Houser, P. R., Arsenault, K. R., Verhoest, N. E., & Pauwels, V. R. (2010). Satellite-scale snow water equivalent assimilation into a high-resolution land surface model. *Journal of Hydrometeorology*, *11*(2), 352–369. doi: 10.1175/2009JHM1192.1

de Rosnay, P., Isaksen, L., & Dahoui, M. (2015). Snow data assimilation at ECMWF. *ECMWF Newsletter*(143), 26–31. doi: 10.21957/lkpxq6x5

Dechant, C., & Moradkhani, H. (2011). Radiance data assimilation for operational snow and streamflow forecasting. *Advances in Water Resources*, *34*(3), 351–364. doi: 10.1016/j.advwatres.2010.12.009

Dee, D. P. (2006). Bias and data assimilation. *Quarterly Journal of the Royal Meteorological Society*, *131*(613), 3323–3343. doi: 10.1256/qj.05.137

de Rosnay, P., Balsamo, G., Albergel, C., Muñoz-Sabater, J., & Isaksen, L. (2014). Initialisation of Land Surface Variables for Numerical Weather Prediction. *Surveys in Geophysics*, *35*(3), 607–621. doi: 10.1007/s10712-012-9207-x

Durand, M., Gatebe, C., Kim, E., Molotch, N., Painter, T., Raleigh, M., ... Vuyovich, C. (2017). NASA SnowEx Science Plan: Assessing Approaches for Measuring Water in Earth's Seasonal Snow. *NASA*, 1–68.

Durand, M., & Margulis, S. A. (2006). Feasibility test of multifrequency radiometric data assimilation to estimate snow water equivalent. *Journal of Hydrometeorology*, *7*(3), 443–457.

Evensen, G. (2003). The Ensemble Kalman Filter: Theoretical formulation and practical implementation. *Ocean Dynamics*, *53*(4), 343–367. doi: 10.1007/s10236-003-0036-9

Gelaro, R., McCarty, W., Suárez, M. J., Todling, R., Molod, A., Takacs, L., ... Zhao, B. (2017). The modern-era retrospective analysis for research and applications, version 2 (MERRA-2). *Journal of Climate*, *30*(14), 5419–5454. doi: 10.1175/JCLI-D-16-0758.1

Getirana, A., Boone, A., Yamazaki, D., Decharme, B., Papa, F., & Mognard, N. (2012). The hydrological modeling and analysis platform (HyMAP): Evaluation in the Amazon basin. *Journal of Hydrometeorology*, *13*(6), 1641–1665. doi: 10.1175/JHM-D-12-021.1

Getirana, A., Kumar, S., Girotto, M., & Rodell, M. (2017). Rivers and Floodplains as Key Components of Global Terrestrial Water Storage Variability. *Geophysical Research Letters*, *44*(20), 10,359–10,368. doi: 10.1002/2017GL074684

Getirana, A., Peters-Lidard, C., Rodell, M., & Bates, P. (2017). Trade-off between cost and accuracy in large-scale surface water dynamic modeling. *Water Resources Research*(53), 4942–4955. doi: 10.1111/j.1752-1688.1969.tb04897.x

Gordon, N., Salmond, D., & Smith, A. (1993). Novel approach to nonlinear Bayesian state estimation. , *140*(2), 107–113.

Griessinger, N., Schirmer, M., Helbig, N., Winstral, A., Michel, A., & Jonas, T. (2019). Implications of observation-enhanced energy-balance snowmelt simulations for runoff modeling of Alpine catchments. *Advances in Water Resources*, *133*(May), 103410. doi: 10.1016/j.advwatres.2019.103410

Grossi, G., Lendvai, A., Peretti, G., & Ranzi, R. (2017). Snow precipitation measured by gauges: Systematic error estimation and data series correction in the central Italian Alps. *Water (Switzerland)*, *9*(7), 1–14. doi: 10.3390/w9070461

Guneriussen, T., Hogda, K. A., Johnsen, H., & Lauknes, I. (2001). InSAR for estimation of changes in snow water equivalent of dry snow. *IEEE Transactions on Geoscience and Remote Sensing*, *39*(10), 2101–2108. doi: 10.1109/36.957273

Hall, D. K., & Riggs, G. A. (2007). Accuracy assessment of the MODIS snow products. *Hydrological Processes*, *21*(November 2008), 1534–1547. doi: 10.1002/hyp.6715

Hedrick, A. R., Marks, D., Havens, S., Robertson, M., Johnson, M., Sandusky, M., ... Painter, T. H. (2018). Direct Insertion of NASA Airborne Snow Observatory-Derived Snow Depth Time Series Into the iSnobal Energy Balance Snow Model. *Water Resources Research*, *54*(10), 8045–8063. doi: 10.1029/2018WR023190

Helfrich, S. R., McNamara, D., Ramsay, B. H., Baldwin, T., & Kasheta, T. (2007). Enhancements to, and forthcoming developments in the Interactive Multisensor Snow and Ice Mapping System (IMS). *Hydrological Processes*, *21*(November 2008), 1576–1586. doi: 10.1002/hyp

Helmert, J., Sorman, A. S., Montero, R. A., De Michele, C., de Rosnay, P., Dumont, M., ... Arslan, A. N. (2018). Review of snow data assimilation methods for hydrological, land surface, meteorological and climate models: Results from a COST harmosnow survey. *Geosciences (Switzerland)*, *8*(12). doi:

10.3390/geosciences8120489

Jordan, R. (1991). A One-dimensional temperature model for a snow cover : technical documentation for SNTHERM.89. *Cold Regions Research and Engineering Laboratory (U.S.)*. doi: http://hdl.handle.net/11681/11677

Jung, H. C., Getirana, A., Policelli, F., McNally, A., Arsenault, K. R., Kumar, S., ... Peters-Lidard, C. D. (2017). Upper Blue Nile basin water budget from a multi-model perspective. *Journal of Hydrology*, *555*, 535–546. doi: 10.1016/j.jhydrol.2017.10.040

Kelly, R. E., Chang, A. T., Tsang, L., & Foster, J. L. (2003). A prototype AMSR-E global snow area and snow depth algorithm. *IEEE Transactions on Geoscience and Remote Sensing*, *41*(2 PART 1), 230–242. doi: 10.1109/TGRS.2003.809118

Krinner, G., Derksen, C., Essery, R., Flanner, M., Hagemann, S., Clark, M., ... Zhu, D. (2018). ESM-SnowMIP: Assessing snow models and quantifying snow-related climate feedbacks. *Geoscientific Model Development*, *11*(12), 5027–5049. doi: 10.5194/gmd-11-5027-2018

Kumar, S. V., Peters-Lidard, C. D., Arsenault, K. R., Getirana, A., Mocko, D., & Liu, Y. (2015). Quantifying the added value of snow cover area observations in passive microwave snow depth data assimilation. *Journal of Hydrometeorology*, *16*(4), 1736–1741. doi: 10.1175/JHM-D-15-0021.1

Kumar, S. V., Peters-Lidard, C. D., Tian, Y., Houser, P. R., Geiger, J., Olden, S., ... Sheffield, J. (2006). Land information system: An interoperable framework for high resolution land surface modeling. *Environmental Modelling and Software*, *21*(10), 1402–1415. doi: 10.1016/j.envsoft.2005.07.004

Kwon, Y., Forman, B. A., Ahmad, J. A., Kumar, S. V., & Yoon, Y. (2019). Exploring the utility of machine learning-based passive microwave brightness temperature data assimilation over terrestrial snow in high Mountain Asia. *Remote Sensing*, *11*(19). doi: 10.3390/rs11192265

Largeron, C., Dumont, M., Morin, S., Boone, A., Lafaysse, M., Metref, S., ... Margulis, S. A. (2020). Toward snow cover estimation in mountainous areas using modern data assimilation methods: A review. *Frontiers in Earth Science*, *8*. Retrieved from `https://www.frontiersin.org/articles/10.3389/feart.2020.00325` doi: 10.3389/feart.2020.00325

Lievens, H., Brangers, I., Marshall, H.-P., Jonas, T., Olefs, M., & De Lannoy, G. (2022). Sentinel-1 snow depth retrieval at sub-kilometer resolution over the European Alps. *The Cryosphere*, *16*(1), 159–177. doi: 10.5194/tc-16-159-2022

Lievens, H., Demuzere, M., Marshall, H.-P., Reichle, R. H., Brucker, L., Brangers, I., ... De Lannoy, G. J. M. (2019). Snow depth variability in the Northern Hemisphere mountains observed from space. *Nature Communications*.

Magnusson, J., Gustafsson, D., Husler, F., & Jonas, T. (2014). Assimilation of point SWE data into a distributed snow cover model comparing two contrasting methods. *Water Resources Research*, *50*, 7816–7835. doi: 10.1002/2014WR015302

Magnusson, J., Winstral, A., Stordal, A. S., Essery, R., & Jonas, T. (2017). Improving physically based snow simulations by assimilating snow depths using the particle filter. *Water Resources Research*(53), 1123–1143. doi: 10.1111/j.1752-1688.1969.tb04897.x

Margulis, S. A., Cortés, G., Girotto, M., & Durand, M. (2016). A landsat-era Sierra Nevada snow reanalysis (1985-2015). *Journal of Hydrometeorology*, *17*(4), 1203–1221. doi: 10.1175/JHM-D-15-0177.1

Marshall, H. P., Deeb, E. J., Lavalle, M., Elder, K., Brucker, L., Hiemstra, C. A., ... Jones, C. (2019). Airborne snow accumulation estimates from L-Band InSAR during the NASA SnowEx 2017 campaign and validation with airborne LiDAR and in-situ observations. *AGU Fall Meeting 2019*.

Mortimer, C., Mudryk, L., Derksen, C., Luojus, K., Brown, R., Kelly, R., & Tedesco,

M. (2019). Evaluation of long term Northern Hemisphere snow water equivalent products. *The Cryosphere Discussions*, 1–24. doi: 10.5194/tc-2019-258

Niu, G. Y., Yang, Z. L., Mitchell, K. E., Chen, F., Ek, M. B., Barlage, M., ... Xia, Y. (2011). The community Noah land surface model with multiparameterization options (Noah-MP): 1. Model description and evaluation with local-scale measurements. *Journal of Geophysical Research Atmospheres*, *116*(12), 1–19. doi: 10.1029/2010JD015139

Oaida, C. M., Reager, J. T., Andreadis, K. M., David, C. H., Levoe, S. R., Painter, T. H., ... Famiglietti, J. S. (2019). A high-resolution data assimilation framework for snow water equivalent estimation across the Western United States and validation with the Airborne Snow Observatory. *Journal of Hydrometeorology*, *20*(3), 357–378. doi: 10.1175/JHM-D-18-0009.1

Painter, T. H., Berisford, D. F., Boardman, J. W., Bormann, K. J., Deems, J. S., Gehrke, F., ... Winstral, A. (2016). The Airborne Snow Observatory: Fusion of scanning lidar, imaging spectrometer, and physically-based modeling for mapping snow water equivalent and snow albedo. *Remote Sensing of Environment*, *184*, 139–152. doi: 10.1016/j.rse.2016.06.018

Park, J., Forman, B. A., & Kumar, S. V. (2022). Estimation of Snow Mass Information via Assimilation of C-Band Synthetic Aperture Radar Backscatter Observations Into an Advanced Land Surface Model. *IEEE Journal of Selected Topics in Applied Earth Observations and Remote Sensing*, *15*, 862-875. doi: 10.1109/JSTARS.2021.3133513

Piazzi, G., Thirel, G., Campo, L., & Gabellani, S. (2018). A particle filter scheme for multivariate data assimilation into a point-scale snowpack model in an Alpine environment. *Cryosphere*, *12*(7), 2287–2306. doi: 10.5194/tc-12-2287-2018

Pivot, F. C. (2012). C-band SAR imagery for snow-cover monitoring at treeline, Churchill, Manitoba, Canada. *Remote Sensing*, *4*(7), 2133–2155. doi: 10.3390/rs4072133

Rasmussen, R., Baker, B., Kochendorfer, J., Meyers, T., Landolt, S., Fischer, A. P., ... Gutmann, E. (2012). How well are we measuring snow: The NOAA/FAA/NCAR winter precipitation test bed. *Bulletin of the American Meteorological Society*, *93*(6), 811–829. doi: 10.1175/BAMS-D-11-00052.1

Reichle, R. H. (2008). Data assimilation methods in the Earth sciences. *Advances in Water Resources*, *31*(11), 1411–1418. doi: 10.1016/j.advwatres.2008.01.001

Reichle, R. H., Liu, Q., Koster, R. D., Draper, C. S., Mahanama, S. P., & Partyka, G. S. (2017). Land Surface Precipitation in MERRA-2. *Journal of Climate*, *30*(5), 1643–1664. doi: 10.1175/JCLI-D-16-0570.1

Reichle, R. H., McLaughlin, D. B., & Entekhabi, D. (2002). Hydrologic data assimilation with the ensemble Kalman filter. *Monthly Weather Review*, *130*(1), 103–114. doi: 10.1175/1520-0493(2002)130⟨0103:HDAWTE⟩2.0.CO;2

Revuelto, J., Cluzet, B., Duran, N., Fructus, M., Lafaysse, M., Cosme, E., & Dumont, M. (2021). Assimilation of surface reflectance in snow simulations: Impact on bulk snow variables. *Journal of Hydrology*, *603*, 126966. Retrieved from `https://www.sciencedirect.com/science/article/pii/S0022169421010167` doi: https://doi.org/10.1016/j.jhydrol.2021.126966

Rott, H., Nagler, T., & Scheiber, R. (2004). Snow mass retrieval by means of SAR interferometry. *European Space Agency, (Special Publication) ESA SP*, *2003*(550), 187–192.

Stigter, E. M., Wanders, N., Saloranta, T. M., Shea, J. M., Bierkens, M. F., & Immerzeel, W. W. (2017). Assimilation of snow cover and snow depth into a snow model to estimate snow water equivalent and snowmelt runoff in a Himalayan catchment. *Cryosphere*, *11*(4), 1647–1664. doi: 10.5194/tc-11-1647-2017

Sun, C., Walker, J. P., & Houser, P. R. (2004). A methodology for snow data as-

680 simulation in a land surface model. *Journal of Geophysical Research D: Atmo-*
681 *spheres*, *109*(8), 1–12. doi: 10.1029/2003JD003765
682 Tarricone, J., Webb, R. W., Marshall, H.-P., Nolin, A. W., & Meyer, F. J. (2022).
683 Estimating snow accumulation and ablation with l-band insar. *The Cryosphere*
684 *Discussions*, *2022*, 1–33. Retrieved from `https://tc.copernicus.org/`
685 `preprints/tc-2022-224/` doi: 10.5194/tc-2022-224
686 Tedesco, M., & Narvekar, P. S. (2010). Assessment of the NASA AMSR-E SWE
687 Product. *IEEE Journal of Selected Topics in Applied Earth Observations and*
688 *Remote Sensing*, *3*(1), 141–159. doi: 10.1109/JSTARS.2010.2040462
689 Toure, A. M., Reichle, R. H., Forman, B. A., Getirana, A., & De Lannoy, G. J. M.
690 (2018). Assimilation of modis snow cover fraction observations into the nasa
691 catchment land surface model. *Remote Sensing*, *10*(2). Retrieved from
692 `https://www.mdpi.com/2072-4292/10/2/316` doi: 10.3390/rs10020316
693 Tsang, L., Durand, M., Derksen, C., Barros, A. P., Kang, D.-H., Lievens, H., ... Xu,
694 X. (2021). Review article: Global monitoring of snow water equivalent using
695 high frequency radar remote sensing. *The Cryosphere Discussions*, *2021*, 1–57.
696 doi: 10.5194/tc-2021-295
697 Wrzesien, M. L., Durand, M. T., & Pavelsky, T. M. (2019). A Reassessment of
698 North American River Basin Cool-Season Precipitation: Developments From
699 a New Mountain Climatology Data Set. *Water Resources Research*, *55*(4),
700 3502–3519. doi: 10.1029/2018WR024106
701 Wrzesien, M. L., Durand, M. T., Pavelsky, T. M., Howat, I. M., Margulis, S. A.,
702 & Huning, L. S. (2017). Comparison of methods to estimate snow wa-
703 ter equivalent at the mountain range scale: A case study of the Califor-
704 nia Sierra Nevada. *Journal of Hydrometeorology*, *18*(4), 1101–1119. doi:
705 10.1175/JHM-D-16-0246.1